Atmos. Chem. Phys. Discuss., 15, 19017–19044, 2015
www.atmos-chem-phys-discuss.net/15/19017/2015/
doi:10.5194/acpd-15-19017-2015

Atmospheric Chemistry and Physics Discussions
Open Access

Constraints on methane emissions in North America from future geostationary remote sensing measurements

N. Bousserez[1], D. K. Henze[1], B. Rooney[1], A. Perkins[4], K. J. Wecht[3], A. J. Turner[3], V. Natraj[2], and J. R. Worden[2]

[1]University of Colorado, Boulder, CO, USA
[2]Jet Propulsion Laboratory, California Institute of Technology, Pasadena, CA, USA
[3]Harvard University, Cambridge, MA, USA
[4]University of Washington, Seattle, WA, USA

Received: 21 April 2015 – Accepted: 13 June 2015 – Published: 10 July 2015

Correspondence to: N. Bousserez (nicolas.bousserez@colorado.edu)

Published by Copernicus Publications on behalf of the European Geosciences Union.

Title Page
Abstract | Introduction
Conclusions | References
Tables | Figures
◂I | I▸
◂ | ▸
Back | Close
Full Screen / Esc
Printer-friendly Version
Interactive Discussion

Abstract

The success of future geostationary (GEO) satellite observation missions depends on our ability to design instruments that address their key scientific objectives. In this study, an Observation System Simulation Experiment (OSSE) is performed to quantify the constraints on methane (CH_4) emissions in North America obtained from Short Wave Infrared (SWIR), Thermal Infrared (TIR) and multi-spectral measurements in geostationary orbit compared to existing SWIR low earth (LEO) measurements. A stochastic algorithm is used to compute the information content of a variational inversion at high spatial resolution ($0.5^{\circ} \times 0.7^{\circ}$) using the GEOS-Chem chemical transport model and its adjoint. Both the SWIR LEO and TIR GEO configurations generally provide poor constraints on CH_4 emissions (error reduction $< 30\,\%$), with the exception of a few hotspots (e.g., Los Angeles, Toronto urban areas and Appalachian Mountains) where the error reduction is greater than 50 %. On weekly time scales and for a GEO orbit, the degree of freedom for signal (DOFs) of the inversion from multi-spectral observations (500) is a factor of two higher than that obtained from a SWIR instrument (255) due to the increase in measurement sensitivity to boundary layer concentrations in the multi-spectral case. On a monthly time scale and for a GEO orbit, a SWIR instrument would reduce error in emission estimates by more than 70 % for hotspots of CH_4 sources (emissions $> 4 \times 10^5\,\mathrm{kg\,day^{-1}\,grid^{-1}}$) at model grid scale, while a TIR instrument would provide a relative error reduction of 25–60 % over those areas. While performing similarly for monthly inversions, a multi-spectral instrument would allow for more than 70 % error reduction for these emissions for 7 or 3 day inversions. Sensitivity of the inversions to error in boundary conditions are found to be negligible. Moreover, estimates of the model resolution matrix over significant emitting regions (CH_4 emissions $> 2 \times 10^5\,\mathrm{kg\,day^{-1}\,grid^{-1}}$) show that for all instrument configurations in GEO orbit the inversion is able to independently constrain CH_4 sources at spatial scales smaller than 200 km. These results highlight the importance of using observations sensitive

to boundary layer concentrations (i.e., SWIR) to achieve significant improvements in constraining CH_4 sources compared to current LEO capabilities.

1 Introduction

Methane (CH_4) plays a key role in both atmospheric chemistry composition and climate. With a radiative forcing relative to preindustrial times that is one third that of carbon dioxide, CH_4 is the second most important greenhouse gas (Myhre, 2013). Further, as a precursor to tropospheric ozone, CH_4 also impacts surface-level air quality (Fiore et al., 2002; West et al., 2006; West and Fiore, 2005), crops (e.g., Shindell et al., 2012) and contributes to ozone radiative forcing (e.g., Fiore et al., 2008). Considerable uncertainty remains in our understanding of CH_4 sources (e.g., Dlugokencky et al., 2011; Kirschke et al., 2013), which include emissions from coal, wetlands, livestock, landfills, biomass burning, geologic seepage, and leaks from the production and distribution of natural gas.

Although there is a growing interest in using CH_4 emission regulations as an efficient lever to simultaneously address current air quality and global warming challenges (e.g., West et al., 2012), the lack of confidence in the available CH_4 emission estimates remains a problematic limitation to design of efficient environmental policies. Indeed, recent studies showed discrepancies of up to a factor of two between bottom-up inventories and top-down inversions using atmospheric CH_4 concentration observations (Katzenstein et al., 2003; Kort et al., 2008; Xiao et al., 2008; Karion et al., 2013; Miller et al., 2013; Wecht et al., 2012; Caulton et al., 2014; Turner et al., 2015; Wecht et al., 2014a). Extrapolation of local emission characteristics to larger areas and/or the use of proxy data (e.g., energy consumption, emission ratios applied to co-emitted species) are the main sources of error in bottom-up methods (Zhen et al., 2015). On the other hand, top-down approaches using space-based measurements of CH_4 from Low Earth Orbit (LEO) platforms allow a global spatial coverage within one to six days but at the same local time. However, as CH_4 emissions can exhibit significant diurnal cycles, e.g., over wetland or boreal peatland (Morin et al., 2014; Gazovic et al., 2010), such temporal under sampling may affect our ability to accurately quantify those fluxes. More generally, insufficient observational coverage and the diffusive nature of transport considerably reduce our ability to spatially resolve grid-scale emissions from space.

Geostationary (GEO) remote-sensing measurements would alleviate the above mentioned shortcomings by providing an almost continuous monitoring and complete spatial coverage of CH_4 concentrations within the field of view. The GEOstationary Coastal and Air Pollution Events (GEO-CAPE) mission (Fishman et al., 2012) was recommended by the National Research Council's Earth Science Decadal Survey in order to improve our understanding of both coastal ecosystems and air-quality from regional to continental scale. Its aim is to enable multiple daily observations of key atmospheric and oceanic constituents over North and South America from a GEO platform. For air-quality applications, such high-spatial and high-temporal-resolution measurements would enable source estimates of air quality pollutants and climate forcers and development of effective emission-control strategies at an unprecedented level of confidence. In order to provide more flexibility and to minimize the cost and risk of the mission, the concept of a phased implementation that would launch remote-sensing instruments separately on commercial host spacecrafts has been adopted. The first phase will consist of the launching of the Tropospheric Emissions: Monitoring of Pollution (TEMPO) instrument circa 2019 (Chance et al., 2013), which will provide GEO hourly measurements of ozone and precursors as well as aerosols over greater North America (from Mexico City to the Canadian tar sands, and from the Atlantic to the Pacific ocean). For the second phase, which aims at completing GEO-CAPE's mission requirements by including measurements of important drivers of climate and air quality such as CH_4, CO, and ammonia (Zhu et al., 2015), a rigorous instrument design study is critical to achieve the mission's scientific objectives within its budget constraints.

In this study we perform an Observation System Simulation Experiment (OSSE) in order to characterize the constraints on grid-scale CH_4 emissions over North America provided by different potential GEO-CAPE instrument configurations. The simulation

ACPD
15, 19017–19044, 2015

consists of a 4D-Var inversion of CH_4 emissions using the GEOS-Chem chemical-transport model (CTM) over a $0.5^{\circ} \times 0.7^{\circ}$ horizontal grid resolution covering North America. In practice, quantifying the information content of such a high-dimensional problem requires either Monte-Carlo simulations or, for linear models, a numerical approximation of the inverse Hessian matrix of the 4D-Var cost function (Tarantola, 2005). The computational cost of Monte-Carlo estimates can be prohibitive, since many perturbed inversions (typically about 50) are needed, each of them usually requiring numerous forward and adjoint model integrations. Therefore, computation of the information content in previous trace-gas Bayesian inversion studies has often relied on explicit calculations of the inverse Hessian matrix, by either considering a regional domain (e.g., Wecht et al., 2014a) or performing a prior dimension reduction of the control vector (e.g., Wecht et al., 2014b; Turner and Jacob, 2015). However, thus far dimension reduction methods for high-dimensional emission inversions have relied on suboptimal criteria.

In this study we use a gradient-based randomization algorithm to approximate the inverse Hessian of the cost function (Bousserez et al., 2015), which allows us to calculate the posterior errors as well as the model resolution matrix (or averaging kernel) of our CH_4 emission inversion at full grid-scale resolution. Such information is used to evaluate the impact of different instrumental designs (spatio-temporal sampling, vertical sensitivity of the measurements) on CH_4 emission constraints. In particular, the potential of CH_4 retrievals from existing Short Wave Infrared (SWIR) and Thermal Infrared (TIR) measurements as well as from a hypothetical multi-spectral instrument on geostationary orbit are examined. Section 2 describes the Observing System Simulation Experiment (OSSE) framework considered in this study, which comprises the 4D-Var method, the forward model, as well as the observations and prior information used. Section 3 presents the results of our experiments, where the information content of the inversion is analyzed in detail. A conclusion to this work is presented in the last section of the paper.

ACPD
15, 19017–19044, 2015

2 Inverse method

2.1 4D-Var system and information content

The variational approach to Bayesian inference is the method of choice for high-dimensional problems, since the solution can be computed by iteratively minimizing a cost function instead of algebraically solving for the minimum, which becomes computationally intractable for high-dimensional systems. Providing the error statistics are all Gaussian, finding the maximum likelihood entails solving the following problem:

$$\arg\min_{\boldsymbol{x}} J(\boldsymbol{x}) \tag{1}$$

$$J(\boldsymbol{x}) = \frac{1}{2}(H(\boldsymbol{x}) - \boldsymbol{y})^T \mathbf{R}^{-1}(H(\boldsymbol{x}) - \boldsymbol{y}) + \frac{1}{2}(\boldsymbol{x} - \boldsymbol{x}_\mathrm{b})^T \mathbf{B}^{-1}(\boldsymbol{x} - \boldsymbol{x}_\mathrm{b}),$$

where $\boldsymbol{x}_\mathrm{b}$ is the prior vector, defined in the control space E of dimension n, $\boldsymbol{x}$ belongs to E, $\boldsymbol{y}$ is the observation vector, defined in the observations vector space F of dimension p, $H : E \rightarrow F$ is the forward model operator (also called observational operator), which associates to any vector in E its corresponding observation in F, and $\mathbf{R}$ and $\mathbf{B}$ are the covariance matrices of the observation and prior errors with dimension $(p \times p)$ and $(n \times n)$, respectively. The argument of the minimum of Eq. (1) is called the analysis and is referred to as $\boldsymbol{x}_\mathrm{a}$.

When the adjoint of the forward model ($\mathbf{H}^T$) is available, the minimum of the cost function J can be found iteratively using a gradient-based minimization algorithm (Lions, 1971). The gradient of the cost function with respect to the control vector $\boldsymbol{x}$ can be written:

$$\nabla J(\boldsymbol{x}) = \mathbf{H}^T \mathbf{R}^{-1}(H(\boldsymbol{x}) - \boldsymbol{y}) + \mathbf{B}^{-1}(\boldsymbol{x} - \boldsymbol{x}_\mathrm{b}). \tag{2}$$

An important result is that if the forward model is approximately linear the posterior error covariance matrix $\mathbf{P}^\mathrm{a}$ is equal to the inverse of the Hessian of the cost function:

$$\mathbf{P}^\mathrm{a} = (\nabla^2 J)^{-1}(\boldsymbol{x}_\mathrm{a}) = (\mathbf{B}^{-1} + \mathbf{H}^T \mathbf{R}^{-1} \mathbf{H})^{-1}. \tag{3}$$

ACPD
15, 19017–19044, 2015

This equivalence can be used to compute information content diagnostics prior to performing the inversion. In this study, following Bousserez et al. (2015), the diagonal elements of $\mathbf{P}^a$ (error variances) are computed using a randomization estimate of $\mathbf{H}^T\mathbf{R}^{-1}\mathbf{H}$. Here an ensemble of 500 random gradients of the cost function are used, based on the convergence of the uniform norm ($\|.\|_\infty$) of the inverse Hessian approximation. Bousserez et al. (2015) showed that good approximation of both the error variances and the error correlations can be obtained using this approach. For the present study we further validated our method by comparing direct finite-difference estimates of selected diagonal elements of $\mathbf{P}^a$ to their stochastic approximations and found a relative error smaller than 10 %.

The model resolution matrix (or averaging kernel $\mathbf{A}$) is defined as the sensitivity of the analysis $\boldsymbol{x}_a$ (optimized CH_4 emissions) to the truth $\boldsymbol{x}_t$ (true emissions):

$$\mathbf{A} \equiv \frac{\partial \boldsymbol{x}_a}{\partial \boldsymbol{x}_t}. \quad (4)$$

The model resolution matrix in Eq. (4) can be rewritten in matrix form:

$$\mathbf{A} = \boldsymbol{I} - \mathbf{P}^a\mathbf{B}^{-1}. \quad (5)$$

Since $\mathbf{B}$ is diagonal in our experiments, Eq. (5) allows us to calculate any element of $\mathbf{A}$ using:

$$\mathbf{A}_{i,j} = \delta_{ij} - \frac{\mathbf{P}^a_{i,j}}{\mathbf{B}_{j,j}}. \quad (6)$$

Finally, the degree of freedom for signal (DOFs) of the inversion is defined as the trace of $\mathbf{A}$, that is: DOFs = $\sum_i \mathbf{A}_{i,i}$.

2.2 Forward model and prior emissions

The forward model in Eq. (1) includes the GEOS-Chem chemistry-transport model, which relates the CH_4 emissions to the 3-D concentration field of atmospheric CH_4, and the satellite observation operator that transforms the CH_4 concentration profiles into their corresponding retrieved profile or columns. The GEOS-Chem simulation used in our experiment is described in (Wecht et al., 2014a; Turner et al., 2015). It consists of a nested simulation over North America at $0.5^\circ \times 0.7^\circ$ horizontal resolution and 72 vertical levels, driven by offline meteorological data provided by GEOS-5 reanalysis from the NASA Global Modeling and Assimilation Office (GMAO). Boundary conditions for the nested domain are used every three hours from a global $4^\circ \times 5^\circ$ GEOS-Chem simulation.

The prior methane emissions we use are from the EDGARv4.2 anthropogenic methane inventory (European Commission, 2011), the wetland model from Kaplan (2002) as implemented by Pickett-Heaps et al. (2011), the GFED3 biomass burning inventory (van der Werf et al., 2010), a termite inventory and soil absorption from Fung et al. (1991), and a biofuel inventory from Yevich and Logan (2003). Figure 1 shows the total average daily prior methane emissions for the entire North America nested domain. Strong hotspots of CH_4 sources clearly appear over the Canadian wetlands, the Appalachian Mountains (an extensive coal mining area) and densely urbanized areas (e.g., southern California and the East Coast). Following previous assessments of the range of the prior error (Wecht et al., 2014a; Turner et al., 2015), we assume a relative prior error of 40 % for our reference case.

2.3 Observations

We consider several instrument configurations for our study, which are associated with different vertical sensitivities. Constraints on CH_4 emissions are evaluated for the following CH_4 retrievals: the Greenhouse gases Observing SATellite (GOSAT) Proxy XCH4 v3.2 data described by Parker et al. (2011) (available from http://www.leos.le.ac.uk/GHG/data/), which consists of CH_4 column mixing ratio X_{CH_4} obtained from Short Wave Infrared (SWIR) measurements near 1.6 µm; the Tropospheric Emission Spectrometer (TES) V005 Lite product (Worden et al., 2012) (http://tes.jpl.nasa.gov/data/), which consists of CH_4 vertical profile retrievals from Thermal Infra Red (TIR) measurements at 7.58–8.55 µm; and a hypothetical multi-spectral CH_4 profile retrievals, which allows for significantly increased sensitivity of the retrieval to boundary layer concentrations. The multi-spectral retrieval are obtained from the 1.6 and 8 µm bands as well as constraints developed for the TES algorithm. The Signal-to-noise ratio (SNR) is then adjusted such that the mapped profile gives a total column that is consistent with the observation error for a GOSAT retrieval. Since the DOFs for the TES retrievals is less than 2, we use an equivalent TES X_{CH_4} column instead of the retrieved CH_4 profiles. Conversely, the multi-spectral retrievals have a DOFs between 2 and 3, and therefore the entire CH_4 profiles were considered for this instrument.

Figure 2 shows the column averaging kernel for the GOSAT and TES X_{CH_4} retrievals as well as the averaging kernels at three different levels for the multi-spectral retrieval. The GOSAT retrieval sensitivity is nearly uniform throughout the troposphere, with averaging kernel values close to 1. The TES retrieval is mostly sensitive to CH_4 concentrations in the upper troposphere, with a peak of the column averaging kernel around 300 hPa. The multi-spectral profile retrieval shows a distinct signal in the boundary layer, with weaker sensitivities above. Observational errors for methane columns (X_{CH_4}) are uniformly set to 8 ppb for both GOSAT and TES. This value is consistent with GOSAT column errors reported in Parker et al. (2011). For the multi-spectral retrieval, a Singular Value Decomposition (SVD) of the covariance matrix of observation errors is performed for each profile in order to decorrelate errors between retrieval levels. As in Wecht et al. (2014b), model transport errors are assumed to be 16 ppb and are added in quadrature with measurement errors. As shown by Locatelli et al. (2013), taking into account transport errors is critical in order to mitigate uncertainties in the inversion, since neglecting them can lead to discrepancies in the posterior estimates of more than 150 % of the prior flux at model grid scale. Finally, contamination by clouds is taken into account for each grid cell by multiplying the corresponding GEOS-5 cloud fraction by the total number of observations within the grid cell and subtracting it from the total number of retrievals.

ACPD
15, 19017–19044, 2015

Both LEO and GEO orbit configurations are also considered in order to assess the relative impact of measurement sensitivity and spatio-temporal sampling on the CH_4 emission constraints. The LEO orbit configuration follows GOSAT's sun-synchronous polar orbit with an Equator overpass local time of ~ 13:00. Measurements consist of five across-track points separated by ~ 100 km, with footprint diameters of 10.5 km. The GEO configuration corresponds to hourly observations over North America from 10 to 60° N. The GEO footprint considered is ~ 4 km, therefore much finer than the GEOS-Chem resolution used (~ 50 km). For both LEO and GEO configurations, observations are therefore averaged together within each GEOS-Chem grid cell and the instrument error is reduced by the square root of the number of observations.

3 Results

In the following experiments, we consider the inversion of 7 or 30 day emission scaling factors. This means that the location and temporal variability of each grid-scale emission is assumed to be known, and only its magnitude is adjusted. The information content of the inversion is analyzed for 4 different observational systems:

- a GOSAT instrument onboard a low-Earth orbit platform (GOSAT_LEO)
- a GOSAT instrument onboard a geostationary orbit platform (GOSAT_GEO)
- a TES instrument onboard a geostationary orbit platform (TES_GEO)
- a multi-spectral instrument onboard a geostationary orbit platform (MULTI_GEO).

3.1 Error reduction of optimized methane emissions

Figure 3 shows the relative error reduction with respect to prior errors achieved by a 7 day inversion, for each of the observational configurations described above. The Degree Of Freedom for Signal (DOFs) is also indicated. The latter quantifies the number of pieces of information independently constrained by the observations. Both the

ACPD
15, 19017–19044, 2015

GOSAT_LEO and TES_GEO observations generally provide poor constraints on North American CH_4 emissions (error reduction < 30 %), with the exception of a few hotspots (e.g., Los Angeles, Toronto urban areas and Appalachian Mountains) where the error reduction is found to be greater than 50 %. The DOFs for those two inversions are comparable (81 and 90 for GOSAT_LEO and TES_GEO, respectively). Much more significant constraints on emissions are obtained from the GOSAT_GEO or MULTI_GEO inversions, for which many locations are found to have error reductions greater than 60 %. Significant error reduction structures can also be seen over western and eastern Canadian wetlands, especially in the case of MULTI_GEO observations. Note that the DOFs for the MULTI_GEO inversion (500) is a factor of two higher than in the GOSAT_GEO case (255), due to the increase in measurement sensitivity to boundary layer concentrations from multi-spectral observations.

Figure 4 shows the relative error reduction from a 30 day inversion for each of the observational configurations. For all configurations, constraints are significantly improved between the 7 and 30 day inversions (DOFs increase by 150 to 250 %), except for the MULTI_GEO case, where the DOFs are similar to the 7 day inversion. This reflects the competitive effects of the increase in the number of observations and the model transport diffusion. While the former tends to increase the amount of available information for each grid point, the latter enhances the smearing of the signal as the inversion time-window expands. Therefore, in the case of a multi-spectral retrieval from geostationary orbit (MULTI_GEO), we find that constraints on the CH_4 emissions are similar between a 7 and a 30 day inversion. Note that Turner et al. (2015) obtained a DOFs of 39 for a multi-year inversion over North America using GOSAT observations. In the latter study, a dimension reduction of the inverse problem was performed in order to optimize the constraints on the emissions and enable an analytical computation of the solution. The DOFs obtained for our 30 day GOSAT_LEO inversion (∼ 200) suggests that the optimal dimension for the inversion is much greater than the one estimated in Turner et al. (2015), and therefore that existing GOSAT observations can constrain many more independent pieces of information than previously thought. The gradient-

ACPD
15, 19017–19044, 2015

based algorithm used in our study allows us to estimate the DOFs of the inversion prior to optimization; this information could be used to objectively determine the appropriate dimension of the inverse problem, upon which specific dimension reduction methods could be devised.

Figure 5 shows the error reduction as a function of emission magnitude, for each observational system and for both 7 and 30 day inversions. Results for a 3 day inversion with MULTI_GEO observations are also shown. As expected, the sensitivity of the error reduction to emission magnitude increases with the length of the inversion time-window. Interestingly, the error reductions achieved by TES_GEO and GOSAT_LEO are found to be similar, which means that using a TIR instrument in geostationary orbit with almost no sensitivity to CH_4 boundary layer concentrations will result in equivalent constraints on emissions as a SWIR instrument on a LEO orbit. This result illustrates the relative importance of the instrument sensitivity to surface concentrations with respect to the temporal sampling of the observations. These results also show that a multi-spectral instrument in GEO orbit would provide significant error reductions (> 60 %) for high CH_4 emissions (> 4.5×10^5 kg day^{-1} grid^{-1}) at time scales as small as 3 days, which would provide useful information on the variability of emissions between workweek and weekend.

3.2 Impact of boundary conditions

As noted Wecht et al. (2014a), a joint inversion of emissions and boundary conditions using satellite measurements may be challenging, since both can theoretically influence the signal in the observations. To remedy that problem, Wecht et al. (2014a) chose to constrain CH_4 emissions and boundary conditions separately, using the same data. This results in the error in emissions being projected onto boundary conditions and vice-versa. Here we evaluate the impact of errors in the boundary condition on the optimized CH_4 emission. Figure 6 shows the response of the optimized CH_4 emissions to a 2 % uniform positive bias in the boundary conditions. The value of the bias has been chosen based on comparisons between simulated GEOS-Chem CH_4 concen-

ACPD
15, 19017–19044, 2015

trations and aircraft-based observations from the HIAPER Pole-to-Pole Observations (HIPPO) experiment (Turner et al., 2015). These results show that a 2 % positive perturbation of the boundary conditions results in absolute posterior emission scaling factor responses smaller than 0.05 for all observational configurations. Moreover, the noisy characteristic of the scaling factor perturbations is evident for all inversions. Therefore, errors in boundary conditions of a few percent or less are found to have a negligible impact on our CH_4 source inversions.

3.3 Spatial resolution of the inversion

An objective measure of the spatial resolution of the inversion, i.e., the ability of the observational system to constrain grid-scale emissions independently from each other, is provided by the rows of the model resolution matrix (see Eq. 5). Figure 7 shows the model resolution matrix rows corresponding to five different locations, chosen to span a range of characteristics, in terms of emissions magnitude and error reduction. Table 1 summarizes the coordinates and CH_4 emissions corresponding to each location. The gain in spatial resolution as the sensitivity of the retrieval to boundary layer CH_4 concentrations increases is evident, especially for eastern Canadian wetlands and the Los Angeles area. For all instrument configurations, observations allow for constraints on CH_4 emissions at spatial resolutions between 80 km × 80 km and 160 km × 160 km. Note that over regions such as the wetlands in eastern Canada, the Appalachian Mountains and the Los Angeles area, using a multi-spectral instrument from geostationary orbit would allow complete constraints of CH_4 sources at grid-scale resolution ($0.5^\circ \times 0.7^\circ$).

4 Conclusions

In this paper we evaluated top-down constraints on methane emissions in North America provided by potential geostationary observation missions (GEO-CAPE) and existing low-earth orbit remote sensing instruments (GOSAT). For the first time, a rigorous es-

ACPD
15, 19017–19044, 2015

timate of the information content of the inversion at high-resolution ($0.5^\circ \times 0.7^\circ$ over North America) in a 4D-Var inversion framework has been performed using an efficient stochastic algorithm. In particular, this allowed us to compute both the relative error reductions and the model resolution matrix (or averaging kernel) of the inversion. Instrument configurations corresponding to current TIR and SWIR methane products (TES and GOSAT, respectively), as well as a potential multi-spectral retrieval, were considered. This allowed us to assess the relative importance of the vertical sensitivity of the measurement and the spatio-temporal resolution of the sampling (GEO vs. LEO) to constrain methane emissions.

Although perfect boundary conditions were assumed, sensitivity tests using an estimated bias of 2 % showed that the impact of errors of this magnitude in boundary conditions on the regional CH_4 inversion was negligible, regardless of the instrument scenario. Both the SWIR LEO and the TIR GEO configurations generally provided poor constraints on CH_4 emissions (error reduction < 30 %), with the exception of a few hotspots (e.g., Los Angeles, Toronto urban areas and Appalachian Mountains) where the error reduction was greater than 50 %. Overall, we found similar constraints from the TIR GEO and SWIR LEO configurations for both 7 and 30 day CH_4 emission inversions, with a DOFs of ~ 80 and ~ 200, respectively. On a weekly time scales and for a GEO orbit, the DOFs of the inversion from multi-spectral observations (500) was a factor of two higher than that obtained from a SWIR instrument (255) due to the increase in measurement sensitivity to boundary layer concentrations in the multi-spectral case. On a monthly time scale and for a GEO orbit, a SWIR instrument reduced emission errors by more than 70 % over hotspots of CH_4 sources (CH_4 emissions $> 4 \times 10^5$ kg day^{-1} grid^{-1}) at model grid scale. Such regions included dense urban areas (e.g., Los Angeles), coal mining over the Appalachian Mountains, or the eastern Canadian wetlands. Comparatively, a TIR GEO instrument provided a relative error reduction of only 25-60 % over those areas, while a multi-spectral GEO instrument allowed for more than 70 % error reduction at 7 or 3 day temporal resolutions. Finally, our estimates of the rows of the model resolution matrix over significant emitting regions

ACPD
15, 19017–19044, 2015

(CH_4 emissions $> 2 \times 10^5$ kg day^{-1} grid^{-1}) showed that, for all instrument configurations in GEO orbit, the inversion was able to independently constrain CH_4 sources at spatial scales smaller than 200 km. In the context of growing concerns about the environmental impacts of CH_4 emissions from oil and gas operations and use, such geostationary observations would provide a key tool to monitor and verify the implementation of regulation strategies. Moreover, they would also allow for better understanding of the critical role of wetlands in the global methane budget and their impact on climate change (e.g., Bloom et al., 2012; Miller et al., 2014). Further investigations would be needed to quantify the sensitivity of these results to the choice of the reference CH_4 emission inventory, since significant discrepancies in the magnitude and spatio-temporal distributions of CH_4 sources exist between current bottom-up estimates (Kirschke et al., 2013).

Acknowledgements. This project was supported by the NASA GEO-CAPE Science Team grant NNX14AH02G. This work utilized the Janus supercomputer, which is supported by the National Science Foundation (award number CNS-0 821 794) and the University of Colorado Boulder. The Janus supercomputer is a joint effort of the University of Colorado Boulder, the University of Colorado Denver and the National Center for Atmospheric Research. Alexander J. Turner was supported by a Department of Energy (DOE) Computational Science Graduate Fellowship (CSGF).

References

Bloom, A. A., Palmer, P. I., Fraser, A., and Reay, D. S.: Seasonal variability of tropical wetland CH_4 emissions: the role of the methanogen-available carbon pool, Biogeosciences, 9, 2821–2830, doi:10.5194/bg-9-2821-2012, 2012. 19031

Bousserez, N., Henze, D. K., Perkins, A., Bowman, K. W., Lee, M., Liu, J., Deng, F., and Jones, D. B. A.: Improved analysis-error covariance matrix for high-dimensional variational inversions: application to source estimation using a 3-D atmospheric transport model, Q. J. Roy. Meteor. Soc., doi:10.1002/qj.2495, 2015. 19021, 19023

Caulton, D. R., Shepson, P. B., Santoro, R. L., Sparks, J. P., Howarth, R. W., Ingraffea, A. R., Cambaliza, M. O., Sweeney, C., Karion, A., Davis, K. J., Stirm, B. H., Montzka, S. A., and

ACPD
15, 19017–19044, 2015

Constraints on methane emissions from geostationary observations

N. Bousserez et al.

Title Page
Abstract | Introduction
Conclusions | References
Tables | Figures
◂ ▸
Back | Close
Full Screen / Esc
Printer-friendly Version
Interactive Discussion

Miller, B. R.: Toward a better understanding and quantification of methane emissions from shale gas development, P. Natl. Acad. Sci. USA, 111, 6237–6242, 2014. 19019
Chance, K., Liu, X., Suleiman, R. M., Flittner, D. E., Al-Saadi, J., and Janz, S. J.: Tropospheric emissions: monitoring of pollution (TEMPO), P. Soc Photo-Opt. Ins., 8866, 88660D, 2013. 19020
Dlugokencky, E. J., Nisbet, E. G., Fisher, R., and Lowry, D.: Global atmospheric methane: budget, changes and dangers, Philos. T. R. Soc. A, 369, 2058–2072, 2011. 19019
Fiore, A. M., Jacob, D. J., Field, B. D., Streets, D. G., Fernandes, S. D., and Jang, C.: Linking ozone pollution and climate change: the case for controlling methane, Geophys. Res. Lett., 29, 25–1, 2002. 19019
Fiore, A. M., West, J. J., Horowitz, L. W., Naik, V., and Schwarzkopf, M. D.: Characterizing the tropospheric ozone response to methane emission controls and the benefits to climate and air quality, J. Geophys. Res.-Atmos., 113, 1984–2012, 2008. 19019
Fishman, J., Iraci, L., Al-Saadi, J., Chance, K., Chavez, F., Chin, M., Coble, P., Davis, C., DiGiacomo, P., Edwards, D., Eldering, L., Goes, J., Herman, J., Hu, C., Jacob, D. J., Jordan, C., Kawa, S. R., Key, R., Liu, X., Lohrenz, S., Mannino, A., Natraj, V., Neil, D., Neu,J., Newchruch, M., Pickering, K., Salisbury, J., Sosik, H., Subramaniam, A., Tzortziou, M., Wang, J., and Wang, M.: The United States' next generation of atmospheric composition and coastal ecosystem measurements: NASA's Geostationary Coastal and Air Pollution Events (GEO-CAPE) Mission, B. Am. Meteorol. Soc., 93, 1547–1566, 2012. 19020
Fung, I., John, J., Lerner, J., Matthews, E., Prather, M., Steele, L., and Fraser, P.: Three-dimensional model synthesis of the global methane cycle, J. Geophys. Res.-Atmos., 96, 13033–13065, 1991. 19024
Gazovic, M., Kutzbach, L., Schreiber, P., Wille, C., and Wilmking, M.: Diurnal dynamics of CH4 from a boreal peatland during snowmelt, Tellus B, 62, 133–139, 2010. 19020
Kaplan, J. O.: Wetlands at the Last Glacial Maximum: distribution and methane emissions, Geophys. Res. Lett., 29, 1079, doi:10.1029/2001GL013366, 2002. 19024
Karion, A., Sweeney, C., Pétron, G., Frost, G., Michael Hardesty, R., Kofler, J., Miller, B. R., Newberger, T., Wolter, S., Banta, R., Brewer, A., Dlugokencky, E., Lang, P., Montzka, S. A., Schnell, R., Tans, P., Trainer, M., Zamora, R., and Conley, S: Methane emissions estimate from airborne measurements over a western United States natural gas field, Geophys. Res. Lett., 40, 4393–4397, 2013. 19019

ACPD
15, 19017–19044, 2015

Constraints on methane emissions from geostationary observations

N. Bousserez et al.

Katzenstein, A. S., Doezema, L. A., Simpson, I. J., Blake, D. R., and Rowland, F. S.: Extensive regional atmospheric hydrocarbon pollution in the southwestern United States, P. Natl. Acad. Sci. USA, 100, 11975–11979, 2003. 19019

Kirschke, S., Bousquet, P., Ciais, P., Saunois, M., Canadell, J. G., Dlugokencky, E. J., Bergamaschi, P., Bergmann, D., Blake, D. P., Bruhwiler, L., Cameron-Smith, P., Castaldi, P., Chevallier, F., Feng, L., Fraser, A., Heimann, M., Hodson, E. L., Houweling, S., Josse, B., Fraser, P. J., Krummel, P. B., Lamarque, J. F., Langenfelds, R. L., Le Quere, C., Naik, V., O'Doherty, S., Palmer, P. I., Pison, I., Plummer, D., Poulter, B., Prinn, R. G., Rigby, M., Ringeval, B., Santini, M., Schmidt, M., Shindell, D. T., Simpson, I. J., Spahni, R., Steele, L. P., Strode, S. A., Sudo, K., Szopa, S., van der Werf, G. R., Voulgarakis, A., van Weele, M., Weiss, R. F., Williams, J. E., and Zen, G.: Three decades of global methane sources and sinks, Nat. Geosci., 6, 813–823, 2013. 19019, 19031

Kort, E. A., Eluszkiewicz, J., Stephens, B. B., Miller, J. B., Gerbig, C., Nehrkorn, T., Daube, B. C., Kaplan, J. O., Houweling, S., and Wofsy, S. C.: Emissions of CH_4 and N_2O over the United States and Canada based on a receptor-oriented modeling framework and COBRA-NA atmospheric observations, Geophys. Res. Lett., 35, 2008. 19019

Lions, J. L.: Optimal Control of Systems Governed by Partial Differential Equations, Springer-Verlag, Berlin, 1971. 19022

Locatelli, R., Bousquet, P., Chevallier, F., Fortems-Cheney, A., Szopa, S., Saunois, M., Agusti-Panareda, A., Bergmann, D., Bian, H., Cameron-Smith, P., Chipperfield, M. P., Gloor, E., Houweling, S., Kawa, S. R., Krol, M., Patra, P. K., Prinn, R. G., Rigby, M., Saito, R., and Wilson, C.: Impact of transport model errors on the global and regional methane emissions estimated by inverse modelling, Atmos. Chem. Phys., 13, 9917–9937, doi:10.5194/acp-13-9917-2013, 2013. 19025

Miller, S. M., Wofsy, S. C., Michalak, A. M., Kort, E. A., Andrews, A. E., Biraud, S. C., Dlugokencky, E. J., Eluszkiewicz, J., Fischer, M. L., Janssens-Maenhout, G., Miller, B. R., Miller, J. B., Montzkad, S. A., Nehrkornf, T., and Sweene, C.: Anthropogenic emissions of methane in the United States, P. Natl. Acad. Sci. USA, 110, 20018–20022, 2013. 19019

Miller, S. M., Worthy, D. E., Michalak, A. M., Wofsy, S. C., Kort, E. A., Havice, T. C., Andrews, A. E., Dlugokencky, E. J., Kaplan, J. O., Levi, P. J., Tian, H., and Zhang, B.: Observational constraints on the distribution, seasonality, and environmental predictors of North American boreal methane emissions, Global Biogeochem. Cy., 28, 146–160, 2014. 19031

Morin, T. H., Bohrer, G., Naor-Azrieli, L., Mesi, S., Kenny, W. T., Mitsch, W. J., and Schaefer, K. V. R.: The seasonal and diurnal dynamics of methane flux at a created urban wetland, Ecol. Eng., 72, 74–83, 2014. 19020

Myhre, G. and Shindell, D.: Climate Change 2013: The Physical Science Basis, Intergovernmental Panel on Climate Change (IPCC), Chap. 8, 2013. 19019

Parker, R., Boesch, H., Cogan, A., Fraser, A., Feng, L., Palmer, P. I., Messerschmidt, J., Deutscher, N., Griffith, D. W., Notholt, J., Wennberg, P. O., and Wunch, D.: Methane observations from the Greenhouse Gases Observing SATellite: comparisonn to ground-based TCCON data and model calculations, Geophys. Res. Lett., 38, L15807, doi:10.1029/2011GL047871, 2011. 19024, 19025

Pickett-Heaps, C. A., Jacob, D. J., Wecht, K. J., Kort, E. A., Wofsy, S. C., Diskin, G. S., Worthy, D. E. J., Kaplan, J. O., Bey, I., and Drevet, J.: Magnitude and seasonality of wetland methane emissions from the Hudson Bay Lowlands (Canada), Atmos. Chem. Phys., 11, 3773–3779, doi:10.5194/acp-11-3773-2011, 2011. 19024

Shindell, D., Kuylenstierna, J. C., Vignati, E., van Dingenen, R., Amann, M., Klimont, Z., Anenberg, S. C., Muller, N., Janssens-Maenhout, G., Raes, F., Schwartz, J., Faluvegi, G., Pozzoli, L., Kupiainen, K., Hoglund-Isaksson, L., Emberson, L., Streets, D., Ramanathan, V., Hicks, K., Oanh, N., Milly, G., Williams, M., Demkine, V., and Fowler, D.: Simultaneously mitigating near-term climate change and improving human health and food security, Science, 335, 183–189, 2012. 19019

Tarantola, A.: Inverse problem theory and methods for model parameter estimation, SIAM, doi:10.1137/1.9780898717921, 2005. 19021

Turner, A. J. and Jacob, D. J.: Balancing aggregation and smoothing errors in inverse models, Atmos. Chem. Phys. Discuss., 15, 1001–1026, doi:10.5194/acpd-15-1001-2015, 2015. 19021

Turner, A. J., Jacob, D. J., Wecht, K. J., Maasakkers, J. D., Biraud, S. C., Boesch, H., Bowman, K. W., Deutscher, N. M., Dubey, M. K., Griffith, D. W. T., Hase, F., Kuze, A., Notholt, J., Ohyama, H., Parker, R., Payne, V. H., Sussmann, R., Velazco, V. A., Warneke, T., Wennberg, P. O., and Wunch, D.: Estimating global and North American methane emissions with high spatial resolution using GOSAT satellite data, Atmos. Chem. Phys. Discuss., 15, 4495–4536, doi:10.5194/acpd-15-4495-2015, 2015. 19019, 19024, 19027, 19029

van der Werf, G. R., Randerson, J. T., Giglio, L., Collatz, G. J., Mu, M., Kasibhatla, P. S., Morton, D. C., DeFries, R. S., Jin, Y., and van Leeuwen, T. T.: Global fire emissions and the

ACPD
15, 19017–19044, 2015

Constraints on methane emissions from geostationary observations

N. Bousserez et al.

contribution of deforestation, savanna, forest, agricultural, and peat fires (1997–2009), Atmos. Chem. Phys., 10, 11707–11735, doi:10.5194/acp-10-11707-2010, 2010. 19024
Wecht, K. J., Jacob, D. J., Wofsy, S. C., Kort, E. A., Worden, J. R., Kulawik, S. S., Henze, D. K., Kopacz, M., and Payne, V. H.: Validation of TES methane with HIPPO aircraft observations: implications for inverse modeling of methane sources, Atmos. Chem. Phys., 12, 1823–1832, doi:10.5194/acp-12-1823-2012, 2012. 19019
Wecht, K. J., Jacob, D. J., Frankenberg, C., Jiang, Z., and Blake, D. R.: Mapping of North American methane emissions with high spatial resolution by inversion of SCIAMACHY satellite data, J. Geophys. Res.-Atmos., 119, 7741–7756, 2014a. 19019, 19021, 19024, 19028
Wecht, K. J., Jacob, D. J., Sulprizio, M. P., Santoni, G. W., Wofsy, S. C., Parker, R., Bösch, H., and Worden, J.: Spatially resolving methane emissions in California: constraints from the CalNex aircraft campaign and from present (GOSAT, TES) and future (TROPOMI, geostationary) satellite observations, Atmos. Chem. Phys., 14, 8173–8184, doi:10.5194/acp-14-8173-2014, 2014b. 19021, 19025
West, J. J. and Fiore, A. M.: Management of tropospheric ozone by reducing methane emissions, Environ. Sci. Technol., 39, 4685–4691, 2005. 19019
West, J. J., Fiore, A. M., Horowitz, L. W., and Mauzerall, D. L.: Global health benefits of mitigating ozone pollution with methane emission controls, P. Natl. Acad. Sci. USA, 103, 3988–3993, 2006. 19019
West, J. J., Fiore, A. M., and Horowitz, L. W.: Scenarios of methane emission reductions to 2030: abatement costs and co-benefits to ozone air quality and human mortality, Clim. Change, 114, 441–461, 2012. 19019
Worden, J., Kulawik, S., Frankenberg, C., Payne, V., Bowman, K., Cady-Peirara, K., Wecht, K., Lee, J.-E., and Noone, D.: Profiles of CH_4, HDO, H_2O, and N_2O with improved lower tropospheric vertical resolution from Aura TES radiances, Atmos. Meas. Tech., 5, 397–411, doi:10.5194/amt-5-397-2012, 2012. 19024
Xiao, Y., Logan, J. A., Jacob, D. J., Hudman, R. C., Yantosca, R., and Blake, D. R.: Global budget of ethane and regional constraints on US sources, J. Geophys. Res.-Atmos., 113, D21, doi:10.1029/2007JD009415, 2008. 19019
Yevich, R. and Logan, J. A.: An assessment of biofuel use and burning of agricultural waste in the developing world, Global Biogeochem. Cy., 17, 1095, doi:10.1029/2002GB001952, 2003. 19024

ACPD
15, 19017–19044, 2015

Constraints on methane emissions from geostationary observations

N. Bousserez et al.

Zhen, L., Pinto, J. P., Turner, A. J., Henze, D. K., Brioude, J., Bousserez, N., Bruhwiler, L. M. P., and Michelsen, H. P.: Mapping methane emissions from oil and natural gas systems in the contiguous United States, Environ. Sci. Technol., submitted, 2015. 19019

Zhu, L., Henze, D., Bash, J. O., Cady-Pereira, K. E., Shephard, M. W., Luo, M., and Capps, S. L.: Sources and impacts of atmospheric NH_3: Current understanding and frontiers for modeling, measurements, and remote sensing in North America, Current Pollution Reports, in press, 2015. 19020

ACPD
15, 19017–19044, 2015

Constraints on methane emissions from geostationary observations

N. Bousserez et al.

Table 1. Coordinates and methane emissions of the five locations considered for the rows of the model resolution matrix.

Region	Coordinates (lon, lat (°))	Emission (10^5 kg day^{-1} grid^{-1})
Eastern US	(−82, 38)	399
Central US	(−104, 40)	830
California	(−117.3, 34.5)	895
Western Canadian Wetlands	(−120, 61.5)	575
Eastern Canadian Wetlands	(−84.6, 52.5)	205

ACPD
15, 19017–19044, 2015
Constraints on methane emissions from geostationary observations
N. Bousserez et al.

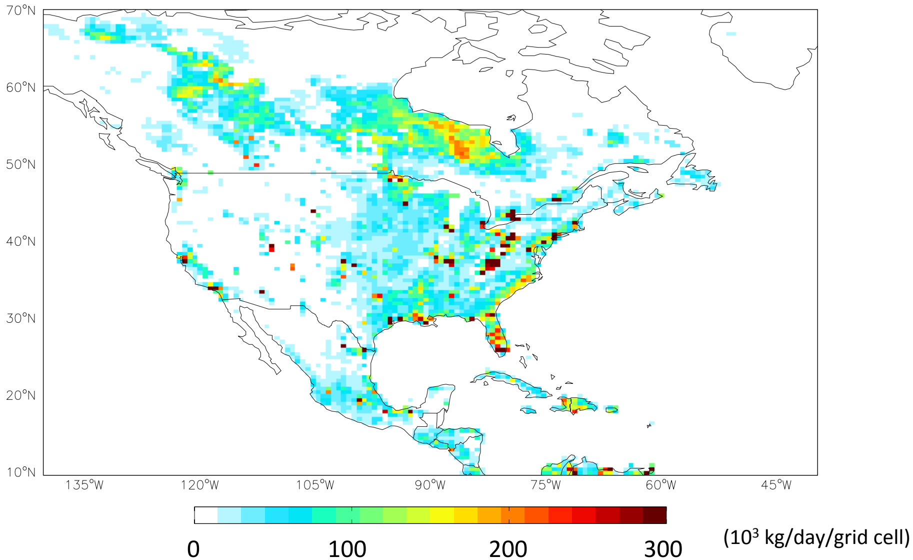

Figure 1. Total average daily prior methane emissions for the nested North America domain (0.5° × 0.7°).

ACPD
15, 19017–19044, 2015

Constraints on methane emissions from geostationary observations

N. Bousserez et al.

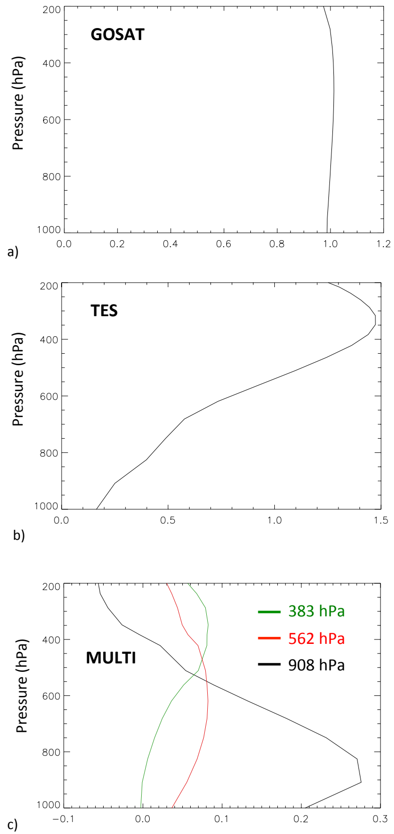

Figure 2. Averaging kernels for the different instrument configurations: **(a)** GOSAT column averaging kernel; **(b)** TES column averaging kernel; **(c)** Multi-spectral averaging kernels at three pressure levels: 908, 562 and 383 hPa.

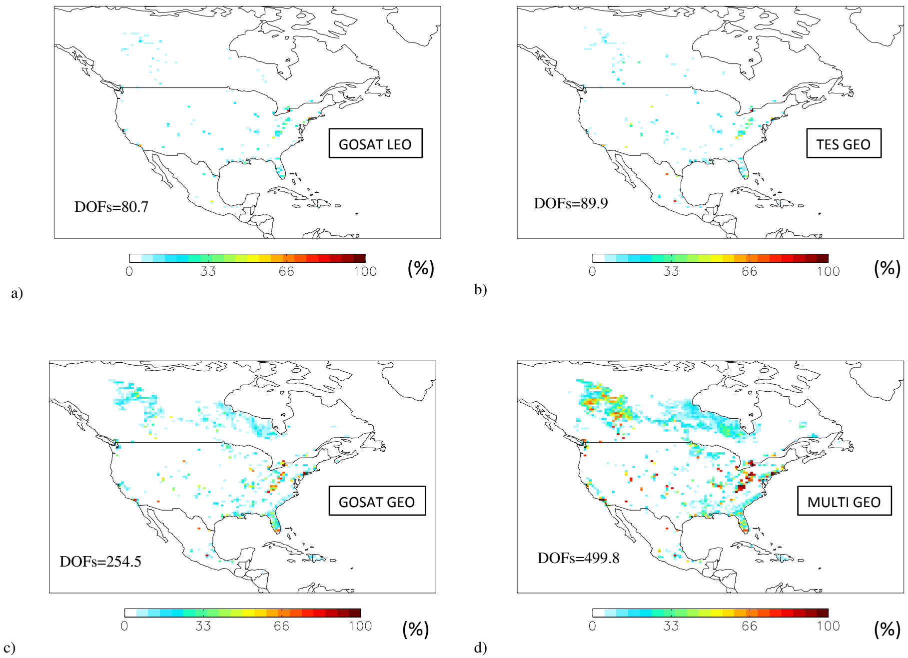

Figure 3. Reduction (%) in methane emission standard errors for a 7 day inversion (1–8 July 2008) using: **(a)** GOSAT low-earth orbit observations (GOSAT_LEO); **(b)** GEO-CAPE observations with a TES-like instrument (TES_GEO); **(c)** GEO-CAPE observations with a GOSAT-like instrument (GOSAT_GEO); **(d)** GEO-CAPE observations with a multi-spectral instrument (MULTI_GEO). The degree of freedom for signal (DOFs) of each inversion is also indicated.

ACPD
15, 19017–19044, 2015

Constraints on methane emissions from geostationary observations

N. Bousserez et al.

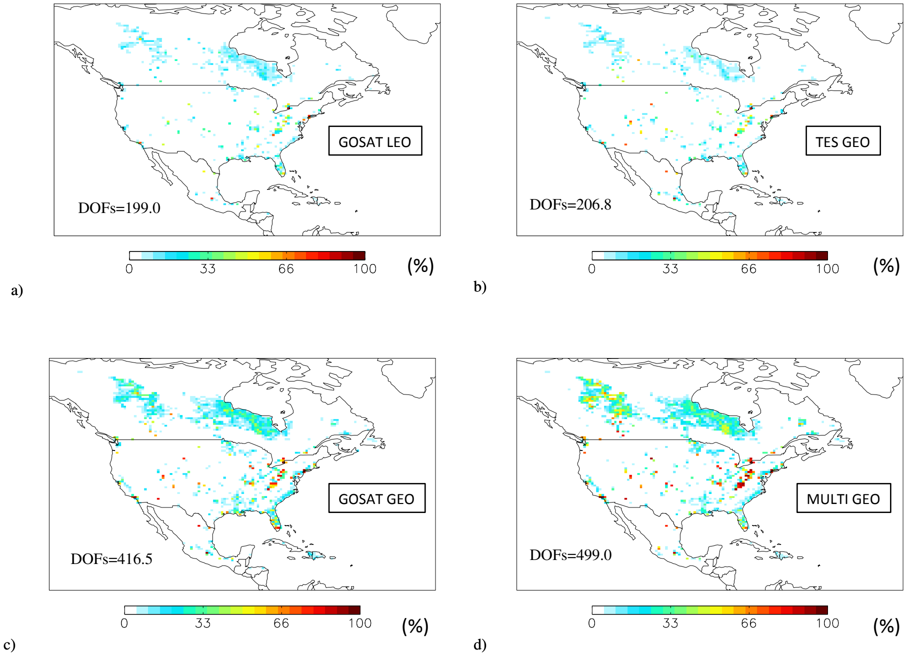

Figure 4. Reduction (%) in methane emission standard errors for a 30 day inversion (1–30 July 2008) using: **(a)** GOSAT low-earth orbit observations (GOSAT_LEO); **(b)** GEO-CAPE observations with a TES-like instrument (TES_GEO); **(c)** GEO-CAPE observations with a GOSAT-like instrument (GOSAT_GEO); **(d)** GEO-CAPE observations with a multi-spectral instrument (MULTI_GEO). The degree of freedom for signal (DOFs) of the inversion is also indicated.

ACPD
15, 19017–19044, 2015

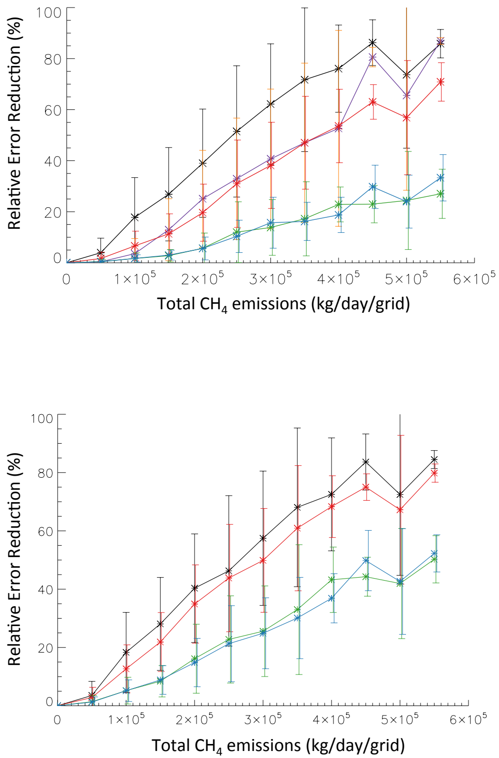

Figure 5. Reduction (%) in methane emission standard errors as a function of emission magnitude for a 7 day (1–8 July 2008) (top) and a 30 day (1–30 July 2008) (bottom) inversion. Blue: GOSAT low-earth orbit observations (GOSAT_LEO); green: GEO-CAPE observations with a TES-like instrument (TES_GEO); red: GEO-CAPE observations with a GOSAT-like instrument (GOSAT_GEO); black: GEO-CAPE observations with a multi-spectral instrument (MULTI_GEO). Results for a 3 day MULTI_GEO inversion are also shown in purple (top). The vertical bars indicate the standard deviation of the relative error reduction within each bin.

ACPD
15, 19017–19044, 2015

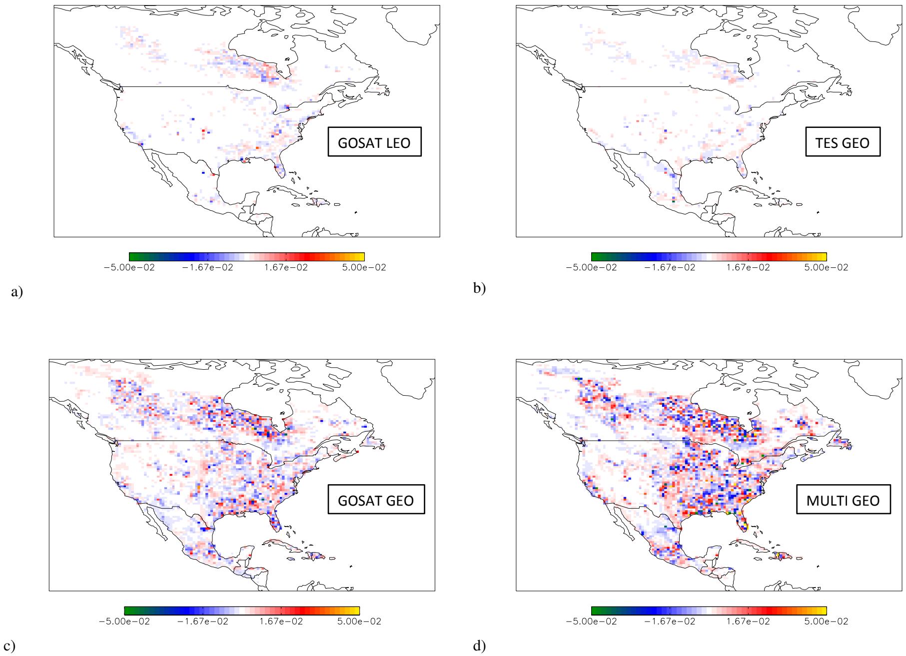

Figure 6. Sensitivity of optimized emission scaling factors (unitless) to a 2 % perturbation of boundary condition methane concentrations for a 30 day inversion (1–30 July 2008), using: **(a)** GOSAT low-earth orbit observations (GOSAT_LEO); **(b)** GEO-CAPE observations with a TES-like instrument (TES_GEO); **(c)** GEO-CAPE observations with a GOSAT-like instrument (GOSAT_GEO); **(d)** GEO-CAPE observations with a multi-spectral instrument (MULTI_GEO).

ACPD
15, 19017–19044, 2015

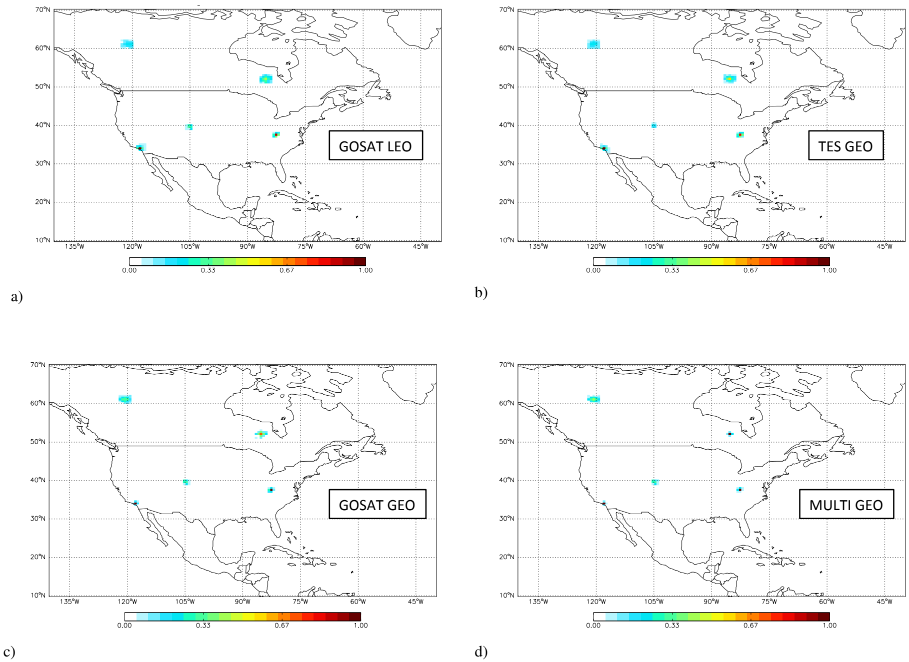

Figure 7. Rows of the model resolution matrix (unitless) for five locations for a 30 day inversion (1–30 July 2008), using: **(a)** GOSAT low-earth orbit observations (GOSAT_LEO); **(b)** GEO-CAPE observations with a TES-like instrument (TES_GEO); **(c)** GEO-CAPE observations with a GOSAT-like instrument (GOSAT_GEO); **(d)** GEO-CAPE observations with a multi-spectral instrument (MULTI_GEO). Coordinates of the five locations considered are reported in Table 1 and correspond to the center of each structure on the maps.

ACPD
15, 19017–19044, 2015